

Observations of the bright radio sources in the North Celestial Pole region at the RATAN-600 radio telescope

M. G. Mingaliev¹, V. A. Stolyarov^{1,2}, R. D. Davies³, S. J. Melhuish⁴, N. A. Bursov¹, and G. V. Zhekanis¹

¹ Special Astrophysical Observatory of Russian Academy of Sciences, Nizhnij Arkhyz,
Karachaev-Cherkessia Republic 357147, Russia

e-mail: marat@sao.ru; vlad@sao.ru; nnb@ratan.sao.ru; gvz@ratan.sao.ru

² University of Cambridge, Institute of Astronomy, Madingley Rd., Cambridge CB3 OHA, UK
e-mail: vlad@ast.cam.ac.uk

³ University of Manchester, Jodrell Bank Observatory, Macclesfield, Cheshire SK11 9DL, UK
e-mail: rdd@jb.man.ac.uk

⁴ University of Wales, Cardiff, Department of Physics and Astronomy, 5, The Parade, Cardiff CF24 3YB, UK
e-mail: Simon.Melhuish@astro.cf.ac.uk

Received 3 November 2000 / Accepted 2 February 2001

Abstract. A survey of the North Celestial Pole region using the RATAN-600 radio telescope at five frequencies in the range 2.3 to 21.7 GHz is described. Sources were chosen from the NVSS catalogue. The flux densities of 171 sources in the Declination range $+75^\circ$ to $+88^\circ$ are presented; typical flux density errors are 5–10 percent including calibration errors. About 20 percent of the sources have flat spectra or a flat component.

Key words. radio astronomy – radio continuum – galaxies

1. Introduction

In the current paper we present the results of observations of bright radio sources in the North Celestial Pole (NCP) region within the declination range of $+75^\circ \leq \delta \leq +88^\circ$ taken with the RATAN-600 radio telescope of the Russian Academy of Sciences (Korolkov & Pariiskii 1979; Parijskij 1993). This NCP survey was initiated as a compliment to the 5 GHz interferometric study of Galactic foreground emission in the NCP made at Jodrell Bank in 1998–1999 (Melhuish et al. 2001). In order to obtain information about Galactic synchrotron and free-free emission in the survey area it was necessary to determine the 5 GHz flux densities of the point sources in the area and remove their contribution from the map.

Up to the present time, there has been no sensitive survey of the NCP region at frequencies higher than the 1.4 GHz NRAO VLA Sky Survey (NVSS), (Condon et al. 1998). The 5 GHz Greenbank survey (Gregory et al. 1996) only extends northwards as far as $\delta = +75^\circ$. There is limited data available at 5 GHz from the early survey at $+88^\circ \leq \delta \leq +90^\circ$ of Pauliny-Toth et al. (1978) and

from the Kuehr et al. (1981) catalogue of bright sources. Furthermore, since a sizable fraction (perhaps as many as 20%) of 5 GHz sources may have flat spectra and are variable, a contemporary survey covering 5 GHz was required for the NCP project. The upper Declination limit of the present RATAN-600 survey was set at $+88^\circ$ since the telescope is used in transit mode and data cannot be collected close to the NCP in this mode.

2. Selection criteria for the survey

The aim of this NCP survey was to obtain information about bright point sources which might make a significant contribution to the 5 GHz degree-scale interferometer survey of foreground Galactic emission in the NCP (Melhuish et al. 2001). The interferometer has a resolution of 2° and a temperature/flux density sensitivity of $60 \mu\text{K}$ in antenna temperature per Jansky. In order to achieve a survey sensitivity approaching $10 \mu\text{K}$ it was decided to measure directly with RATAN-600 all those sources giving $10 \mu\text{K}$ or more with the interferometer, corresponding to a flux density $S \geq 150 \text{ mJy}$. At this flux density there is one source per interferometer beam area of $2^\circ \times 2^\circ$.

Table 1. Parameters of the receivers used in the survey. See text for meaning of the symbols

ν_c , GHz	$\Delta\nu$, GHz	ΔT , mK	T_{phys} , K	T_{ampl} , K	T_{sys} , K
21.7	2.5	3.5	15	23	77
11.2	1.4	3.0	15	18	70
7.7	1.0	3.0	15	14	62
3.9	0.6	2.5	15	8	37
2.3	0.4	8.0	310	35	95

The sources chosen for measurement were taken from the 1.4 GHz NVSS catalogue, the catalogue covering the NCP region which is nearest in frequency to 5 GHz. A 150 mJy flux density limit at 5 GHz corresponds to 350–400 mJy at 1.4 GHz assuming an average spectral index of 0.7 ($S \propto \nu^{-\alpha}$) for the sources. Accordingly, the adopted “complete sample” criteria for the sources selected from the NVSS catalogue were:

1. Flux density $S_\nu \geq 400$ mJy at the NVSS frequency of 1.4 GHz;
2. $00^\circ \leq \alpha \leq 24^\circ$;
3. $+75^\circ \leq \delta \leq +88^\circ$.

In total we have selected for observation 182 objects which satisfy these criteria.

3. The observations

The observations were made in February-March 1999 using the South sector of the RATAN-600 reflector – type radio telescope at 2.3, 3.9, 7.7, 11.2 and 21.7 GHz (Parijskij 1993; Berlin et al. 1997; Berlin & Friedman 1996). The parameters of the receivers are listed in Table 1, where ν_c is the central frequency, $\Delta\nu$ is the bandwidth, ΔT is the sensitivity of the radiometer over 1 s integration, T_{phys} is the physical temperature of the radiometer amplifier, T_{ampl} is the noise temperature of the amplifier and T_{sys} is the noise temperature of the whole system at the given frequency. All of the radiometers have HEMT first-stage amplifiers.

Information about $FWHM$ can be found in the article by Kovalev et al. (1999). For example at 11.2 GHz the $FWHM$ is about $17'' \times 2'$ at the elevations of the NCP observations.

Usually each source was observed 5–8 times per set. Scans of all of the sources were corrected for baseline slope when fitted to a Gaussian response using data reduction software developed by Verkhodanov (1997). The accuracy of the antenna temperature of each source was determined as the standard error of the mean from the N observations of the set.

4. Calibration and data reduction

The calibration of our observations is a challenging task. There are no radio astronomical calibrators listed in this area of the sky. The only place where we have some information about source fluxes in a wide frequency range

(0.325–42 GHz) in the NCP region is the VLA Calibrator List (Perley & Taylor 1999). However, the fluxes listed there are approximate because most of the sources from the VLA List are compact and, hence, variable. To address this problem we selected for our purpose only sources with steep spectra that are not likely to be variable and, if possible, with minimal expected VLA amplitude closure errors (about 3%). The fluxes of the calibrators from the VLA Calibrator List are listed at 90, 20, 6, 3.7, 2 and 0.7 cm wavelength bands (0.325, 1.5, 5, 8.1, 15 and 42.9 GHz respectively). In order to get fluxes at the RATAN-600 frequency bands the spectra of the calibrators were interpolated to the desired frequencies by second order polynomial.

4.1. The calibration errors, σ_c

The flux density measurement procedure at the RATAN-600 is described by Aliakberov et al. (1985). The response of the antenna to a source with known flux density at a given frequency ν is a function of antenna elevation (Mingaliev et al. 1998), which may be expressed as:

$$T_{\text{ant},\nu} = F_\nu(S_\nu, e) = S_\nu f_\nu(e) \quad S_\nu = T_{\text{ant},\nu} g_\nu(e), \quad (1)$$

where

$$\begin{aligned} g_\nu(e) &= 1/f_\nu(e) && \text{- elevation calibration function;} \\ T_{\text{ant},\nu} & && \text{- antenna temperature;} \\ F_\nu, f_\nu & && \text{- arbitrary functions;} \\ e = 90 - \phi + \delta & && \text{- antenna elevation;} \\ \phi = 43^\circ 65333 & && \text{- latitude of the telescope site.} \end{aligned}$$

In order to get the flux density from $T_{\text{ant},\nu}$ we have to multiply it by the elevation calibration function $g_\nu(e)$, which is believed to be a second order polynomial (Trushkin 1985). To get an estimate of this function we observe the calibration sources of known flux density spanning a wide range of declination, δ . Having the list of values

$$g_\nu(e_i) = S_{\nu,i}/T_{\text{ant},\nu,i}$$

for different sources we can approximate the functions $g_\nu(e)$ by a second order polynomial with the help of minimization of the mean square value of the estimated error (least square estimator).

The names of calibration sources we used and their adopted flux densities are listed in the Table 2. The assumed flux density errors are 3% as given in the VLA Calibrator List.

The calibration curves $g_\nu(e)$ for 2.3, 3.9, 7.7 and 11.2 GHz are given in Fig. 1. A second order polynomial fit was made to the observational data at each frequency. We found the errors in the calibration curves were 11, 10.3, 2.4, 5.6 and 7.4% at 21.7, 11.2, 7.7, 3.9 and 2.3 GHz respectively. The total calibration error is the quadratic addition of the 3% VLA Calibration List error and the error from the $g_\nu(e)$ calibration curve.

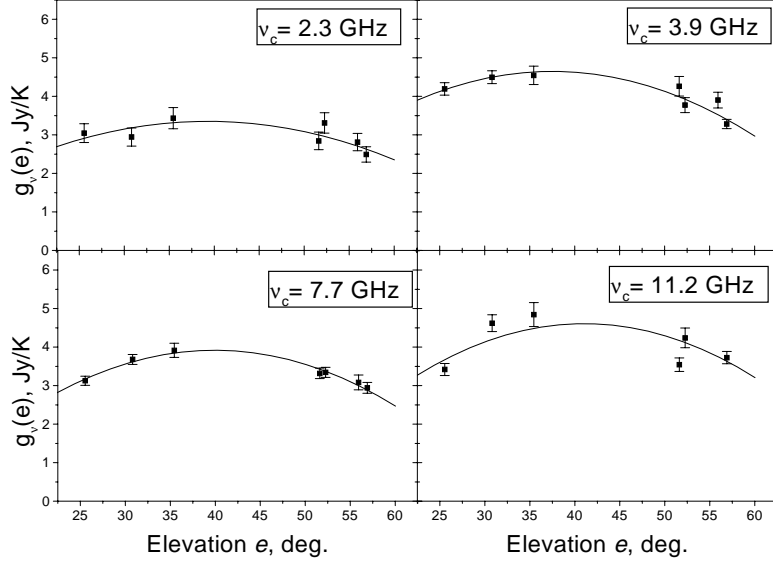


Fig. 1. Calibration curves for 2.3, 3.9, 7.7 and 11.2 GHz bands

Table 2. Adopted calibrator source flux densities. Sources are from the VSA Calibrator List; errors are assumed to be 3%

Name of the source	$S(\nu_c = 21.7 \text{ GHz}),$ Jy	$S(\nu_c = 11.2 \text{ GHz}),$ Jy	$S(\nu_c = 7.7 \text{ GHz}),$ Jy	$S(\nu_c = 3.9 \text{ GHz}),$ Jy	$S(\nu_c = 2.3 \text{ GHz}),$ Jy
J0017+815	0.48	0.78	0.94	1.00	0.9
J0229+777	–	–	0.41	1.05	1.8
J0410+769	1.14	1.77	2.23	3.35	4.49
J0626+820	0.31	0.56	0.74	1.01	0.95
J1435+760	–	0.31	0.44	0.74	1.03
J1459+716	1.00	1.72	2.27	3.69	5.33
J2022+761	0.42	0.41	0.43	0.44	0.46

4.2. The errors of T_{ant} measurements, σ_m

The specifics of the RATAN-600 observations lead to the fact that the errors of the antenna temperature measurements depend not only on the receiver noise, but also on the atmospheric fluctuations on the scale of the main beam, on the accuracy of antenna surface setting for the actual source observation and on the accuracy of the feed cabin positioning (the cabin with secondary mirror and receivers).

Generally speaking, the part of these errors due to the receiver noise can be estimated according to the formula

$$\Delta T_{\text{rec}} = \Delta T / (\Delta t N k)^{1/2} \quad (2)$$

where ΔT is the sensitivity of the receiver over 1 s (listed in Table 1); Δt is an integration time, the time that the source takes to cross the main beam of the antenna during the drift scan; N is the number of the drift scans; k is equal to 1 for single horn receivers (2.3 and 3.9 GHz) and 2 for beam-switching receivers (7.7, 11.2, 21.7 GHz), where we can take into account both positive and negative beams. The variable parameter is Δt , because it depends on the width of the main beam which is different for different frequencies, and varies with declination. In the case of the NCP declination range and the frequency range 21.7 to 2.3 GHz, Δt lies in the range 1–15 s. As an example for

3.9 GHz, $\delta = +75^\circ$, $\Delta t = 4$ s and $N = 5$, ΔT_{rec} is equal to 0.56 mK.

Unfortunately the contribution of atmospheric fluctuations increases as Δt increases corresponding to larger angular scales thereby partially reducing the growth of sensitivity expected from longer integration times. The errors related to the accuracy of antenna surface setting and feed cabin positioning are more complicated to account for. The feed cabin position errors are most important for high frequency observations; as an example it is necessary to position the cabin with an accuracy of 0.1λ , which is 1.4 mm in the case of 21.7 GHz.

However, estimating of the antenna temperature of the source for every drift scan (e.g by Gaussian fitting) and then calculating the variance of the T_{ant} for the N observations of the data set can give us the measurement error, σ_m , including all of the components listed above.

4.3. The total errors, σ_t

The total fractional error in the flux densities listed in this survey is the quadratic sum of the total calibration error

and the error in the antenna temperature measurement, namely,

$$\left(\frac{\sigma_t}{S_\nu}\right)^2 = \left(\frac{\sigma_c}{g_\nu(e)}\right)^2 + \left(\frac{\sigma_m}{T_{ant,\nu}}\right)^2 \quad (3)$$

where

σ_t	- total standard error;
σ_c	- standard error of calibration;
σ_m	- standard error of $T_{ant,\nu}$ measurement;
S_ν	- flux density;
$g_\nu(e) = 1/f_\nu(e)$	- elevation calibration function;
$T_{ant,\nu}$	- antenna temperature.

The values of the standard error of $T_{ant,\nu}$ measurement, σ_m , are 2–3% for 11.2, 7.7 and 3.9 GHz, 3–5% for 2.3 GHz and 7–11% for 21.7 GHz. For the brighter sources σ_m is typically half these values, indicating highly consistent observations. Thus at the frequencies of 21.7, 11.2 and 3.9 GHz the calibration errors dominate.

4.4. Comparison with the other catalogues

The RATAN-600 results described in this paper are in good accordance with the flux densities given by NVSS at 1.4 GHz, the Westerbork Northern Sky Survey (WENSS; Rengelink et al. 1997) at 0.325 GHz and the earlier data of the Kuehr (1981) Catalogue. Four sample spectra are shown in Fig. 2 which compare the RATAN-600 data with those from the three above catalogues. The sources illustrated all have steep spectra and as a consequence are not likely to be variable. The few discrepancies in the plotted spectra are all in the older Kuehr data.

5. Results

The spectra for 171 sources in the present RATAN-600 NCP survey are given in Table 4. Data from WENSS and NVSS are included. Nearly all the sources have complete data at 2.3, 3.9, 7.7 and 11.2 GHz; 40 sources have 21.7 GHz flux densities. Only a few of these sources have been observed previously over this wide frequency range. The columns in the table are:

- Column 1:* The source name (NVSS notation), corresponding to epoch J2000 coordinates;
- Columns 2–3:* The flux density in Jy and standard error at 0.325 GHz (WENSS catalogue, Rengelink et al. 1997);
- Columns 4–5:* The flux density in Jy and standard error at 1.4 GHz (NVSS catalogue, Condon et al. 1998);
- Columns 6–15:* The flux density in Jy and total standard error, σ_t , at 2.3, 3.9, 7.6, 11.2 and 21.7 GHz respectively;
- Column 16:* The spectral index $\alpha = -\log(S(\nu_1)/S(\nu_2))/\log(\nu_1/\nu_2)$, computed between fluxes at 0.325 and 11.2 GHz (or the nearest available frequencies).

A number of the sources in the NVSS target list were not fully resolved in the RATAN-600 observations, largely as a result of the more extended beam in the declination direction. These closely adjacent sources are listed as a single entry in Table 4 and are designated as RAXXX and DecXXX. The listed flux densities of these complexes are the sum of the flux densities of the individual sources. The NVSS sources contributing to each of the 7 complexes are given in Table 3.

6. Discussion

Some preliminary comments are worthwhile on the multi-frequency data for this NCP survey in which 171 individual sources were identified.

6.1. The contribution to 5 GHz interferometry

The first aim of these observations was to obtain a list of those sources which would contribute at a significant level to our 5 GHz survey (Melhuish et al. 2001) of the NCP. The chosen limit to the flux density at 5 GHz was 150 mJy which corresponds to a signal amplitude of 10 μ K in the interferometer. The majority of sources (80 percent) were stronger than this limit and would make a significant contribution to the CMB foreground and should be removed from the interferometer survey.

The question then arises as to the further contribution from flat spectrum and rising spectrum sources not included in our survey which would have a 5 GHz flux density of ≥ 150 mJy. Remembering that our source selection criterion was 400 mJy at 1.4 GHz, a spectral index of 0.7 gives a flux density of 150 mJy at 5 GHz. A source spectral index of 0.2 will give twice this limit; only 10 percent of our sources chosen at 1.4 GHz have spectral indices flatter than this value. Accordingly there will be a further contribution from such sources with flux densities at 1.4 GHz of 200–400 mJy. Assuming the fraction of flat spectrum sources stays constant with decreasing frequency, we may expect ~ 5 sources in this category. Yet another contribution will come from Gigahertz Peaked Spectrum (GPS) sources; likewise there will be ~ 5 extra sources with a flux density above 150 mJy at 5 GHz.

6.2. Statistics of sources spectra

Although this is a modest sample of GHz spectra, it provides an indication of the spectral properties of the brightest radio sources in the NCP region ($+75^\circ \leq \delta \leq +88^\circ$). We would expect them to follow the trends in the general field. One particular advantage of the present catalogue is that all the sources were observed simultaneously at all frequencies to provide an instantaneous spectrum unaffected by source variability. The histograms of spectral index values estimated over the frequency ranges 0.325/1.4 GHz, 0.325/3.9 GHz, 3.9/11.2 GHz and 0.325/11.2 GHz are presented in Figs. 3–6 respectively.

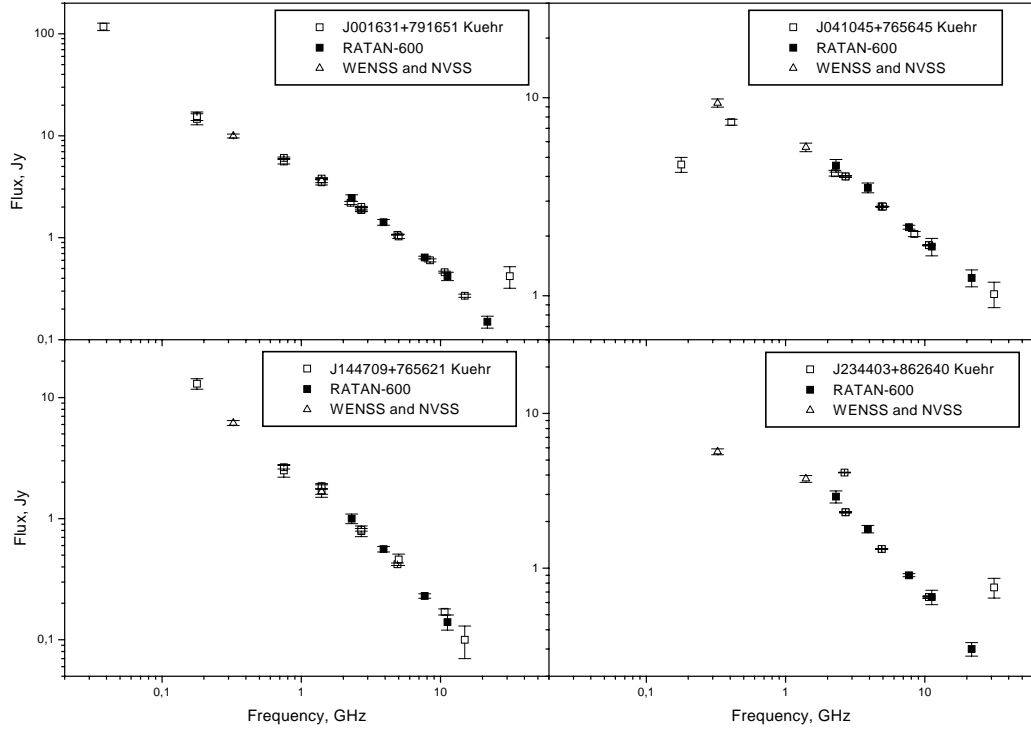


Fig. 2. Four sample source spectra from Kuehr catalogue compared with RATAN-600, NVSS and WENSS data

Table 3. Complex sources

Name in NVSS	Name in the Table 4	Name in NVSS	Name in the Table 4
J022235+861727	J0222XX+861XXX	J184142+794752	J184XXX+794XXX
J022248+861851		J184151+794727	
J022249+862027		J184214+794613	
J074246+802741	J074XXX+802XXX	J184226+794517	
J074305+802544		J204257+750428	J20425X+750XXX
J101330+855411	J101XXX+855XXX	J204259+750306	
J101412+855349		J211814+751203	J2118XX+751XXX
		J211817+751112	
		J235521+795552	J2355XX+795XXX
		J235525+795442	

The majority of the sources have spectral indices in the range 0.6 to 1.5 at GHz frequencies. The canonical steepening of synchrotron spectra at higher frequencies is evident in the data. The median spectral index in the range 0.325/1.4 GHz is 0.78. This value rises to 0.82 for 1.4/2.3 GHz, to 0.95 for 2.3/3.9 GHz and to 1.15 for 3.9/11.2 GHz. At the higher part of this frequency range there is an increasing spread in the range of spectral indices which indicates that the turn-over of the spectrum occurs at a range of GHz frequencies. This broadening of the histogram is readily seen in Fig. 5 where a significant number (~ 30 percent) have a spectral index greater than 1.2 in the frequency range 3.9/11.2 GHz; a small fraction (~ 10 percent) of these higher spectral indices are a result of the significant total error, σ_t , on weaker sources at 11.2 GHz.

The fraction of flatter spectrum sources in our GHz NCP survey, as illustrated in Figs. 4–6, is 20–25 percent. This family of flattish spectrum sources is of particular concern as a foreground in the measurement of fluctuations in the cosmic microwave background.

6.3. Individual sources with compact components

The spectral signature of compact radio sources is a flat component arising from synchrotron self-absorption. Such a component may be seen as a flat spectrum over a wide frequency range, a flat spectrum component at a high frequency emerging from a steep spectrum low-frequency source or a GHz Peaked Spectrum source. Such spectra are found in some 20 percent of the 171 sources of the present survey. 14 sources show a relatively flat spectrum over the

Table 4. Fluxes of the sources in the NCP region

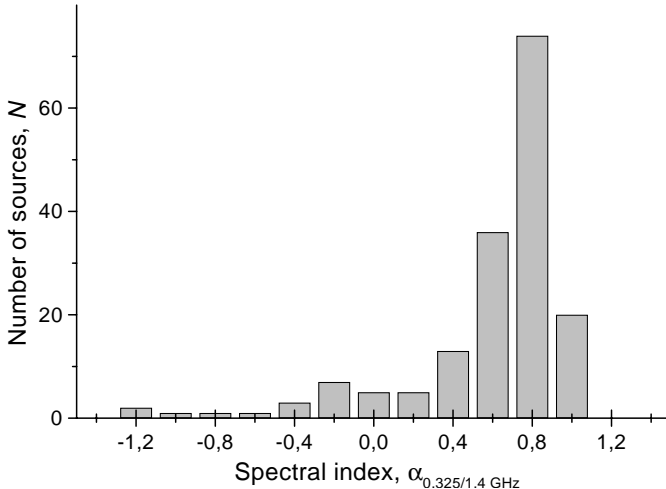
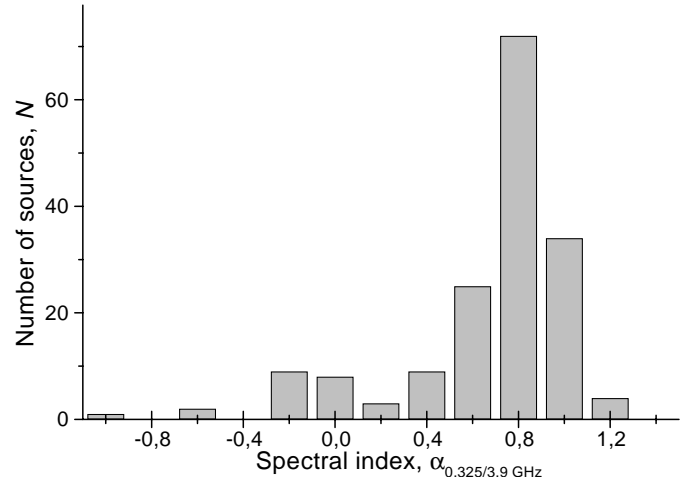
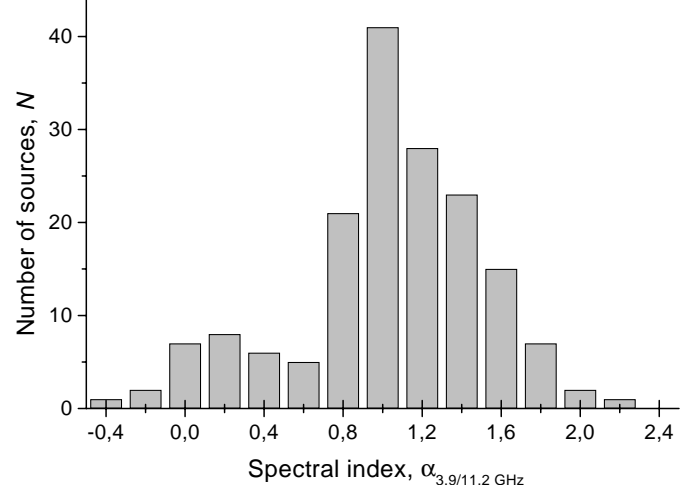
Name, NVSS	$S_{0.325}$ Jy,	σ_t WENSS	$S_{1.4}$ Jy,	σ_t NVSS	$S_{2.3}$ Jy	σ_t	$S_{3.9}$ Jy	σ_t	$S_{7.7}$ Jy	σ_t	$S_{11.2}$ Jy	σ_t	$S_{21.7}$ Jy	σ_t	Sp. index $\alpha_{0.325/11.2}$
J000943+772440	2.059	0.082	0.628	0.021	0.447	0.04	0.267	0.017	0.161	0.007	0.14	0.016	—	—	0.76
J001236+854313	1.605	0.064	0.691	0.023	0.539	0.048	0.246	0.018	0.148	0.005	0.099	0.011	—	—	0.79
J001311+774846	4.517	0.181	2.101	0.071	1.578	0.141	0.981	0.056	0.467	0.012	0.314	0.034	0.202	0.03	0.75
J001631+791651	9.959	0.398	3.651	0.123	2.46	0.183	1.422	0.087	0.643	0.017	0.422	0.044	0.145	0.022	0.89
J001708+813508	0.688	0.028	0.693	0.023	0.853	0.067	1.022	0.058	0.919	0.023	0.788	0.082	0.441	0.065	-0.04
J001816+782743	2.16	0.086	0.707	0.024	0.428	0.038	0.252	0.015	0.109	0.005	0.054	0.006	—	—	1.04
J003812+844727	0.972	0.039	0.406	0.014	0.332	0.03	0.223	0.017	0.108	0.005	0.084	0.01	—	—	0.69
J004617+751752	1.371	0.055	0.444	0.015	0.273	0.025	0.163	0.012	0.074	0.004	0.04	0.005	—	—	1
J011045+873822	2.215	0.089	0.686	0.023	0.467	0.042	0.206	0.015	0.118	0.005	0.081	0.009	—	—	0.93
J013156+844612	2.072	0.083	0.777	0.026	0.603	0.054	0.361	0.027	0.186	0.005	0.136	0.016	—	—	0.77
J015207+755035	2.823	0.113	0.839	0.028	0.526	0.047	0.285	0.016	0.095	0.005	0.054	0.006	—	—	1.12
J020537+752207	0.86	0.035	1.151	0.039	0.873	0.078	0.611	0.036	0.309	0.009	0.202	0.021	0.097	0.015	0.41
J020723+795602	3.89	0.156	1.363	0.046	0.932	0.072	0.582	0.033	0.252	0.008	0.18	0.021	—	—	0.87
J0222XX+861XXX	20.538	0.822	6.478	0.217	4.006	0.422	3.006	0.261	1.137	0.133	0.813	0.095	—	—	0.91
J022454+765554	5.949	0.238	1.927	0.065	1.271	0.095	0.744	0.042	0.334	0.009	0.21	0.023	0.085	0.013	0.94
J022914+774316	8.067	0.323	2.683	0.09	1.663	0.124	0.95	0.054	0.401	0.011	0.259	0.028	0.111	0.016	0.97
J023010+814129	2.285	0.091	1.048	0.035	0.783	0.07	0.544	0.031	0.284	0.008	0.213	0.023	0.212	0.031	0.67
J025100+791359	2.475	0.099	0.713	0.024	0.475	0.043	0.226	0.013	0.089	0.003	0.036	0.004	—	—	1.2
J025417+791147	2.186	0.088	0.643	0.022	0.463	0.041	0.212	0.013	0.105	0.006	0.067	0.008	—	—	0.98
J030011+820238	2.415	0.097	1.379	0.046	1.078	0.102	0.586	0.034	0.265	0.008	0.177	0.022	—	—	0.74
J030454+772731	0.164	0.008	0.977	0.033	0.926	0.07	0.634	0.036	0.344	0.009	0.262	0.028	0.157	0.024	-0.13
J035150+800437	1.534	0.061	0.546	0.018	0.368	0.033	0.211	0.012	0.078	0.004	0.041	0.005	—	—	1.02
J035446+800929	1.243	0.05	0.644	0.022	0.499	0.045	0.371	0.023	0.279	0.008	0.259	0.028	0.211	0.031	0.44
J035629+763742	1.969	0.079	0.629	0.021	0.397	0.036	0.252	0.016	0.127	0.007	0.098	0.011	—	—	0.85
J035817+783719	1.334	0.053	0.508	0.017	0.367	0.033	0.226	0.016	0.102	0.003	0.065	0.007	—	—	0.85
J040652+763354	1.592	0.064	0.527	0.018	0.384	0.034	0.195	0.012	0.095	0.004	0.068	0.008	—	—	0.89
J041045+765645	9.406	0.376	5.62	0.189	4.538	0.336	3.512	0.197	2.215	0.054	1.769	0.182	1.279	0.142	0.47
J041426+761243	1.359	0.054	0.405	0.014	0.259	0.023	0.147	0.011	0.061	0.003	0.04	0.005	—	—	1
J041531+842457	1.965	0.079	0.578	0.019	0.453	0.041	0.235	0.015	0.128	0.004	0.09	0.01	—	—	0.87
J041946+755915	1.491	0.06	0.427	0.014	0.273	0.025	0.166	0.01	0.076	0.004	0.045	0.005	—	—	0.99
J042205+762708	3.75	0.15	1.043	0.035	0.598	0.053	0.309	0.018	0.1	0.006	0.05	0.006	—	—	1.22
J042408+765341	1.614	0.065	0.408	0.014	0.223	0.02	0.146	0.011	0.035	0.002	0.019	0.002	—	—	1.25
J042918+770911	4.702	0.188	0.945	0.032	0.517	0.044	0.266	0.015	0.085	0.004	0.026	0.003	—	—	1.47
J044545+783856	1.807	0.072	0.65	0.022	0.46	0.041	0.292	0.022	0.156	0.004	0.113	0.013	0.068	0.01	0.78
J050731+791257	1.859	0.074	0.629	0.021	0.496	0.044	0.307	0.019	0.155	0.004	0.122	0.014	0.066	0.01	0.77
J050842+843204	0.149	0.007	0.295	0.01	0.302	0.031	0.242	0.019	0.246	0.008	0.25	0.027	0.169	0.025	-0.15
J061837+782123	2.511	0.101	1.075	0.036	0.733	0.066	0.501	0.038	0.227	0.012	0.119	0.014	—	—	0.86
J062205+871948	2.105	0.084	0.645	0.022	0.534	0.048	0.251	0.019	0.1	0.006	0.072	0.008	—	—	0.95
J062602+820225	0.199	0.009	0.681	0.023	0.962	0.086	0.947	0.054	0.763	0.019	0.717	0.074	0.521	0.06	-0.36
J063012+763245	2.187	0.088	0.783	0.026	0.7	0.063	0.339	0.025	0.152	0.009	0.092	0.011	—	—	0.9
J063012+763245	1.512	0.061	0.481	0.016	—	—	0.193	0.015	0.085	0.004	0.053	0.006	—	—	0.95
J063825+841106	3.834	0.153	1.1	0.037	0.737	0.066	0.426	0.029	0.197	0.005	0.155	0.018	—	—	0.91
J064045+781327	1.605	0.064	0.688	0.023	0.403	0.036	0.249	0.018	0.092	0.004	0.048	0.005	—	—	0.99
J064558+775502	2.054	0.082	0.608	0.02	0.458	0.041	—	—	0.098	0.006	0.067	0.008	—	—	0.97
J071452+815153	1.704	0.068	0.551	0.018	0.419	0.037	0.255	0.016	0.141	0.004	0.127	0.014	—	—	0.73
J072611+791130	0.092	0.005	0.501	0.017	0.75	0.057	0.904	0.051	0.818	0.02	0.742	0.077	0.48	0.054	-0.59
J073433+765813	1.361	0.055	0.475	0.016	0.282	0.025	0.217	0.013	0.098	0.006	0.074	0.009	—	—	0.82
J074XXX+802XXX	9.574	0.383	3.322	0.112	2.408	0.185	1.699	0.124	0.954	0.05	0.681	0.076	—	—	0.75
J075058+824158	3.741	0.15	1.845	0.062	1.579	0.119	1.421	0.08	0.959	0.024	0.881	0.091	0.643	0.095	0.41
J080626+812620	1.506	0.06	0.406	0.014	0.251	0.023	0.127	0.008	0.045	0.002	0.033	0.004	—	—	1.08
J080734+784610	1.574	0.063	0.525	0.018	0.39	0.035	0.218	0.013	0.106	0.003	0.084	0.01	—	—	0.83
J082550+765313	1.903	0.076	0.689	0.023	0.491	0.044	0.303	0.018	0.159	0.004	0.121	0.014	0.028	0.004	0.78
J083236+800601	2.019	0.081	0.867	0.029	0.638	0.057	0.392	0.023	0.184	0.005	0.132	0.015	0.051	0.008	0.77
J084833+783003	5.369	0.215	1.509	0.051	0.86	0.077	0.508	0.029	0.203	0.006	0.127	0.014	0.038	0.006	1.06
J085834+750121	0.239	0.01	0.948	0.032	0.578	0.052	0.302	0.017	0.097	0.006	0.048	0.005	—	—	0.45
J090112+780930	1.422	0.057	0.447	0.015	0.252	0.023	0.165	0.012	0.069	0.003	0.059	0.007	—	—	0.9
J090842+834543	1.039	0.042	0.448	0.015	0.325	0.029	0.221	0.013	0.118	0.003	0.099	0.011	—	—	0.66
J092016+862845	2.122	0.085	0.519	0.017	0.345	0.031	0.173	0.013	0.065	0.003	0.036	0.004	—	—	1.15
J093239+790629	9.234	0.369	2.241	0.075	1.333	0.119	0.667	0.038	0.235	0.006	0.127	0.014	—	—	1.21
J093817+781528	2.062	0.083	0.699	0.023	0.426	0.038	0.272	0.016	0.125	0.004	0.075	0.009	—	—	0.94
J093923+831526	11.592	0.464	2.953	0.099	1.802	0.134	0.917	0.052	0.304	0.009	0.171	0.02	—	—	1.19
J094440+825408	1.904	0.076	0.735	0.025	0.54	0.048	0.358	0.023	0.173	0.006	0.129	0.015	—	—	0.76
J095559+791134	1.295	0.052	0.415	0.014	0.254	0.023	0.152	0.009	0.061	0.003	0.047	0.005			

Table 4. continued

1	2	3	4	5	6	7	8	9	10	11	12	13	14	15	16
J105150+791341	1.894	0.076	0.525	0.018	0.314	0.028	0.179	0.01	0.078	0.004	0.06	0.007	–	–	0.98
J110405+793253	0.338	0.014	0.514	0.017	0.491	0.044	0.377	0.021	0.237	0.006	0.172	0.018	0.11	0.016	0.19
J110412+765859	7.554	0.302	2.341	0.079	1.518	0.113	0.887	0.05	0.395	0.01	0.224	0.023	–	–	0.99
J111342+765449	1.534	0.061	0.471	0.016	0.29	0.026	0.183	0.011	0.095	0.005	0.066	0.007	–	–	0.89
J112342+773123	1.516	0.061	0.407	0.014	0.228	0.02	0.151	0.009	0.055	0.003	0.036	0.004	–	–	1.06
J114829+782721	0.97	0.039	0.42	0.014	0.3	0.027	0.206	0.012	0.088	0.005	0.074	0.009	–	–	0.73
J115312+805829	1.39	0.056	1.343	0.045	1.887	0.146	1.922	0.108	1.715	0.042	1.696	0.175	1.251	0.138	-0.06
J115504+753439	1.822	0.073	0.817	0.027	0.594	0.053	0.407	0.025	0.201	0.006	0.137	0.016	–	–	0.73
J115522+815709	2.017	0.081	0.671	0.023	0.428	0.038	0.227	0.019	0.1	0.004	0.065	0.007	–	–	0.97
J115608+823505	1.4	0.056	0.404	0.014	0.25	0.023	0.175	0.02	0.065	0.003	0.056	0.007	–	–	0.91
J115713+811824	1.269	0.051	0.981	0.033	0.766	0.06	0.556	0.033	0.301	0.009	0.222	0.023	–	–	0.49
J122015+792732	1.409	0.056	0.517	0.017	0.334	0.03	0.214	0.012	0.084	0.004	0.043	0.005	–	–	0.99
J122340+804004	1.204	0.048	0.705	0.024	0.701	0.063	0.752	0.043	0.767	0.019	0.808	0.083	0.775	0.087	0.11
J122518+860839	1.532	0.061	0.453	0.015	0.294	0.026	0.164	0.016	0.082	0.004	0.041	0.005	–	–	1.02
J123708+835704	1.909	0.076	0.778	0.026	0.667	0.051	0.333	0.02	0.186	0.005	0.122	0.014	–	–	0.78
J125736+834231	1.145	0.046	0.475	0.016	0.375	0.034	0.27	0.019	0.176	0.005	0.164	0.019	–	–	0.55
J130035+805438	4.837	0.194	1.251	0.042	0.777	0.069	0.386	0.022	0.166	0.004	0.107	0.012	–	–	1.08
J130538+815626	1.734	0.069	0.49	0.016	0.32	0.029	0.17	0.01	0.077	0.004	0.054	0.006	–	–	0.98
J130609+800825	2.218	0.089	0.785	0.026	0.597	0.053	0.365	0.022	0.18	0.007	0.142	0.016	–	–	0.78
J130705+764918	1.178	0.047	0.754	0.025	0.531	0.048	0.359	0.021	0.18	0.006	0.124	0.014	–	–	0.64
J130811+854424	1.711	0.069	0.593	0.02	0.418	0.037	0.236	0.015	0.156	0.009	0.108	0.012	–	–	0.78
J131723+821916	3.126	0.125	0.869	0.029	0.46	0.041	0.29	0.017	0.114	0.007	0.08	0.009	–	–	1.04
J132053+845011	0.702	0.028	0.436	0.015	0.484	0.044	0.28	0.021	0.211	0.007	0.189	0.022	–	–	0.37
J132145+831613	0.829	0.033	0.565	0.019	0.485	0.043	0.333	0.025	0.275	0.015	0.262	0.03	–	–	0.33
J132331+780947	1.192	0.048	0.482	0.016	0.346	0.031	0.23	0.014	0.106	0.003	0.072	0.008	–	–	0.79
J132351+794251	0.574	0.023	0.599	0.02	0.642	0.057	0.575	0.033	0.476	0.012	0.435	0.046	0.331	0.042	0.08
J135639+794340	2.121	0.085	0.579	0.019	0.349	0.031	0.189	0.011	0.072	0.004	0.036	0.004	–	–	1.15
J135755+764320	0.419	0.017	0.647	0.022	0.575	0.051	0.7	0.04	0.769	0.02	0.819	0.085	0.761	0.085	-0.19
J141419+790547	1.445	0.058	0.424	0.014	0.251	0.023	0.153	0.01	0.082	0.004	0.056	0.007	–	–	0.92
J141718+805939	1.519	0.061	0.541	0.018	0.356	0.032	0.217	0.016	0.115	0.005	0.077	0.009	–	–	0.84
J141947+760033	3.216	0.129	0.981	0.033	0.635	0.057	0.388	0.022	0.192	0.007	0.137	0.016	0.058	0.009	0.89
J142248+770416	1.094	0.044	0.541	0.018	0.329	0.029	0.173	0.01	0.063	0.003	0.029	0.003	–	–	1.03
J142613+794607	1.257	0.05	0.407	0.014	0.266	0.024	0.168	0.012	0.067	0.003	0.036	0.004	–	–	1
J143547+760526	2.644	0.106	1.304	0.044	0.979	0.087	0.724	0.041	0.428	0.011	0.323	0.034	0.191	0.028	0.59
J144314+770726	6.648	0.266	1.882	0.063	1.069	0.095	0.552	0.034	0.225	0.006	0.131	0.015	–	–	1.11
J144709+765621	6.168	0.247	1.667	0.056	0.997	0.089	0.559	0.032	0.226	0.006	0.144	0.016	–	–	1.06
J150008+751851	3.858	0.154	0.784	0.026	0.395	0.035	0.19	0.011	0.076	0.004	0.044	0.005	–	–	1.26
J150207+860811	0.863	0.035	0.416	0.014	0.379	0.034	0.229	0.014	0.108	0.003	0.087	0.01	–	–	0.65
J151304+814326	2.144	0.086	0.782	0.026	0.554	0.05	0.302	0.022	0.134	0.004	0.088	0.01	–	–	0.9
J153112+770604	1.446	0.058	0.566	0.019	0.346	0.031	0.18	0.01	0.056	0.003	0.021	0.002	–	–	1.2
J153700+815431	0.2	0.009	0.433	0.015	0.39	0.035	0.314	0.018	0.2	0.005	0.163	0.019	0.095	0.014	0.06
J160222+801558	4.507	0.18	1.016	0.034	0.515	0.046	0.255	0.015	–	–	0.049	0.005	–	–	1.28
J160929+793954	2.806	0.112	1.239	0.042	0.965	0.086	0.711	0.04	0.431	0.012	0.333	0.035	0.193	0.028	0.6
J161940+854921	3.965	0.159	1.643	0.055	1.322	0.098	0.801	0.046	0.433	0.011	0.319	0.034	–	–	0.71
J163051+823345	–	–	0.875	0.029	0.378	0.034	0.259	0.019	0.086	0.005	0.052	0.006	–	–	1.36
J163226+823220	–	–	0.802	0.027	0.777	0.064	0.644	0.037	0.555	0.014	0.615	0.065	0.647	0.096	0.13
J163925+863153	2.234	0.089	0.852	0.029	0.633	0.057	0.418	0.026	0.233	0.006	0.173	0.019	–	–	0.72
J164843+754628	5.799	0.232	1.942	0.065	1.246	0.111	0.746	0.042	0.365	0.01	0.245	0.026	0.109	0.016	0.89
J165752+792808	2.458	0.098	0.872	0.029	0.599	0.054	0.399	0.024	0.179	0.006	0.123	0.014	–	–	0.85
J171416+761245	1.916	0.077	0.459	0.015	0.268	0.024	0.139	0.008	0.056	0.003	0.031	0.004	–	–	1.17
J172359+765312	0.216	0.009	0.424	0.014	0.342	0.03	0.358	0.02	0.343	0.011	0.315	0.033	0.279	0.042	-0.11
J172529+770805	0.979	0.039	0.565	0.019	0.425	0.038	0.262	0.016	0.134	0.005	0.096	0.011	–	–	0.66
J172550+772624	3.077	0.123	1.163	0.039	0.795	0.071	0.499	0.028	0.27	0.007	0.206	0.023	0.132	0.019	0.76
J173021+794916	4.444	0.178	1.02	0.034	0.648	0.058	0.309	0.033	0.126	0.004	0.064	0.007	–	–	1.2
J173734+844453	1.971	0.079	0.444	0.015	0.258	0.023	0.128	0.009	0.054	0.003	0.029	0.003	–	–	1.19
J175056+814736	1.139	0.046	0.44	0.015	0.269	0.024	0.161	0.011	0.054	0.003	0.033	0.004	–	–	1
J180045+782804	1.918	0.077	2.224	0.075	2.679	0.205	2.883	0.162	2.674	0.067	2.69	0.278	2.427	0.272	-0.1
J183712+851449	1.852	0.074	0.69	0.023	0.526	0.047	0.246	0.016	0.113	0.004	0.057	0.007	–	–	0.98
J184XXX+794XXX	30.187	1.207	12.944	0.435	9.44	0.859	5.94	0.416	3.63	0.37	–	–	–	–	0.85
J184502+765230	1.517	0.061	0.536	0.018	0.347	0.031	0.251	0.016	0.101	0.006	0.061	0.007	–	–	0.91
J185750+774636	1.636	0.066	0.474	0.016	0.291	0.026	0.166	0.01	0.074	0.004	0.042	0.005	–	–	1.03
J190350+853647	2.533	0.101	0.905	0.03	0.63	0.056	0.411	0.03	0.192	0.005	0.147	0.017	–	–	0.8
J190919+781330	0.823	0.033	0.465	0.016	0.33	0.03	0.202	0.012	0.094	0.003	0.057	0.007	–	–	0.75
J193419+795606	2.721	0.109	0.765	0.026	0.518	0.046	0.231	0.016	0.101	0.006	0.049	0.005	–	–	1.13
J193739+835629	0.844	0.034	0.43	0.014	0.392	0.035	0.239	0.015	0.22	0.008	0.265	0.028	–	–	0.33
J194136+850138	2.477	0.099</td													

Table 4. continued

1	2	3	4	5	6	7	8	9	10	11	12	13	14	15	16
J204541+762510	3.238	0.13	0.953	0.032	0.603	0.054	0.474	0.027	0.257	0.008	0.201	0.023	–	–	0.79
J205033+752622	2.107	0.084	0.556	0.019	0.365	0.032	0.182	0.012	0.082	0.004	0.046	0.005	–	–	1.08
J210407+763307	15.52	0.621	3.891	0.131	2.27	0.169	1.314	0.074	0.486	0.012	0.259	0.027	–	–	1.16
J2118XX+751XXX	4.717	0.189	1.261	0.042	0.66	0.059	0.419	0.027	0.135	0.004	0.078	0.009	–	–	1.16
J211956+765734	1.188	0.048	0.432	0.015	0.307	0.027	0.15	0.011	0.082	0.004	0.05	0.006	–	–	0.89
J212926+845326	3.514	0.141	1.274	0.043	0.809	0.072	0.482	0.035	0.168	0.007	0.072	0.008	–	–	1.1
J213008+835730	5.098	0.204	1.798	0.06	1.332	0.119	0.846	0.048	0.382	0.01	0.279	0.032	–	–	0.82
J213139+843011	0.445	0.018	0.677	0.023	0.647	0.058	0.422	0.032	0.241	0.007	0.185	0.021	–	–	0.25
J213334+823905	1.93	0.077	0.915	0.031	0.809	0.072	0.617	0.035	0.433	0.01	0.39	0.045	0.192	0.028	0.45
J213929+833953	1.418	0.057	0.48	0.016	0.306	0.027	0.217	0.012	0.107	0.006	0.081	0.009	–	–	0.81
J214928+754045	1.735	0.069	0.524	0.018	0.329	0.029	0.202	0.012	0.104	0.006	0.073	0.009	–	–	0.9
J215657+833714	0.474	0.019	0.474	0.016	0.442	0.039	0.285	0.022	0.214	0.009	0.184	0.021	–	–	0.27
J215712+764642	2.283	0.091	0.777	0.026	0.56	0.05	0.309	0.018	0.149	0.006	0.091	0.011	–	–	0.91
J220955+835356	1.787	0.072	0.578	0.019	0.4	0.036	0.191	0.018	0.09	0.005	0.069	0.008	–	–	0.92
J222800+753219	2.039	0.082	0.651	0.022	0.429	0.038	0.289	0.018	0.142	0.005	0.111	0.013	–	–	0.82
J224714+855542	1.432	0.057	0.516	0.017	0.356	0.032	0.205	0.013	0.098	0.006	0.076	0.009	–	–	0.83
J230122+795406	1.447	0.058	0.431	0.014	0.291	0.026	0.154	0.01	0.077	0.004	0.044	0.005	–	–	0.99
J230138+820015	1.518	0.061	0.45	0.015	0.378	0.034	0.196	0.016	0.085	0.004	0.046	0.005	–	–	0.99
J232503+791715	0.705	0.028	1.136	0.038	0.912	0.082	0.578	0.037	0.285	0.007	0.189	0.021	–	–	0.37
J232640+823158	2.964	0.119	1.001	0.034	0.728	0.065	0.35	0.022	0.16	0.009	0.066	0.007	–	–	1.07
J232803+761738	1.466	0.059	0.459	0.015	0.26	0.023	0.172	0.01	0.072	0.004	0.053	0.006	–	–	0.94
J234403+822640	5.667	0.227	3.777	0.127	2.904	0.259	1.787	0.102	0.896	0.022	0.65	0.067	0.292	0.043	0.61
J234914+751744	1.428	0.057	0.43	0.014	0.322	0.029	0.2	0.013	0.117	0.007	0.096	0.011	–	–	0.76
J235413+804753	1.634	0.065	0.482	0.016	0.307	0.027	0.178	0.01	0.075	0.004	0.058	0.007	–	–	0.94
J2355XX+795XXX	6.463	0.259	1.706	0.057	0.967	0.073	0.603	0.034	0.196	0.007	0.094	0.011	–	–	1.2
J235622+815252	0.569	0.023	0.521	0.017	0.454	0.041	0.5	0.032	0.586	0.016	0.667	0.071	0.713	0.08	-0.04

**Fig. 3.** Spectral index distribution between 0.325 and 1.4 GHz**Fig. 4.** Spectral index distribution between 0.325 and 3.9 GHz**Fig. 5.** Spectral index distribution between 3.9 and 11.2 GHz

whole frequency range measured; of these, 4 show weak GPS behavior (see below) and 3 show weakly rising spectra up to the highest frequency observed and may also be GPS sources. 4 sources show evidence for a flat spectrum component at the higher frequencies of the survey.

There is a potential 10 percent of this survey which are GPS sources. These are believed to be compact objects with a peak in their spectra at GHz frequencies in the redshift frame of emission. They are characterized by a difference of spectral index (“curvature”) on either side of the peak of more than 0.6 (de Vries et al. 1997). The observed peak frequency may be as low as 0.5 GHz (Marecki et al. 1999). There are 9 sources in our list which satisfy these spectral characteristics. It is possible that several may be giant radio galaxies with low frequency absorption (for

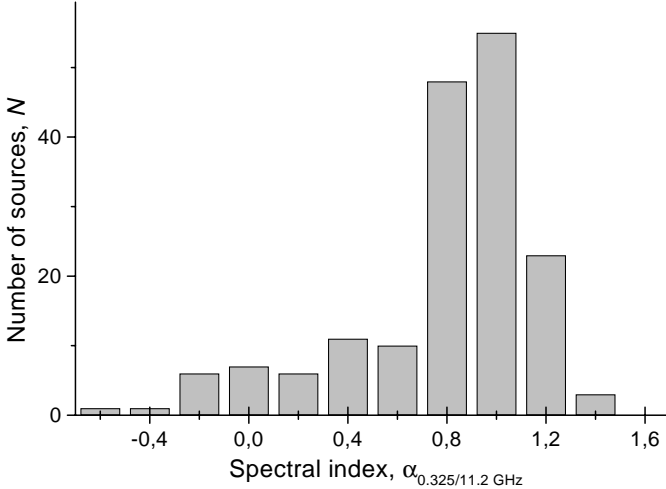


Fig. 6. Spectral index distribution between 0.325 and 11.2 GHz

example 085834+750121); mapping will be required to establish their compactness. Four sources (132351+794251; 172359+765312; 180045+782804; 200531+775243) have a curvature of 0.4 to 0.6, just below the canonical limit of de Vries et al.; they are compact as indicated by their spectra and are potential GPS sources. Three sources (104423+805439; 135755+764320; 235622+815252) have spectra which are weakly rising with $\alpha = 0.2$ to 0.3 at the highest frequencies of observation. These are also likely GPS sources with peak frequencies ≥ 10 to 20 GHz.

Acknowledgements. This research is partially supported by the Russian Foundation for Basis Research Project No. 98-02-16428 and Russian Federal Program “Astronomy” Project No. 1.2.5.1. VS acknowledges the receipt of NATO/Royal Society Postdoctoral Fellowship.

The authors used extensively the database CATS (<http://cats.sao.ru>, Verkhodanov et al. 1997) of the Special Astrophysical Observatory (Russia) in the search for counterparts in the radio catalogues.

References

- Aliakberov, K., Mingaliev, M., Naugol'naya, M., et al. 1985, *Astrophys. Issled. (Izvestiya SAO)*, 19, 60
- Berlin, A., & Friedman, P. 1996, Real Time Radiometric Data Processing Against Electromagnetic Pollution, in 25th General Assembly of the International Union of Radio Science abstracts, Lille, France, 750
- Berlin, A., Maksysheva, A., Nizhelskij, N., et al. 1997, Spread spectrum radiometers of RATAN-600 radio telescope, in The problems of Modern Radio Astronomy, 27th Radio Astronomy Conference, Sankt-Peterburg, 115
- Condon, J. J., Cotton, W. D., Greisen, E. W., et al. 1998, AJ, 115, 1693
- Giardino, G., Asareh, H., Melhuish, S. J., et al. 2000, MNRAS, 313, 689
- Gregory, P. C., Scott, W. K., Douglas, K., & Condon, J. J. 1996, ApJS, 103, 427
- Korolkov, D. V., & Pariiskii, Yu. N. 1979, *Sky Telesc.*, 57, 324
- Kovalev, Y. Y., Nizhelsky, N. A., Kovalev, Yu. A., et al. 1999, A&AS, 139, 545
- Kuehr, H., Witzel, A., Pauliny-Toth, I. I. K., & Nauber, U. 1981, A&AS, 45, 367
- Marecki, A., Falcke, H., Niezgoda, J., Garrington, S. T., & Patnaik, A. R. 1999, A&AS, 135, 273
- Melhuish, S. J., Davies, R. D., Mingaliev, M. G., & Stolyarov, V. A. 2001, in preparation
- Mingaliev, M., Botashev, A., & Stolyarov, V. 1998, Multi-frequency monitoring of a sample of extragalactic radio sources, In IAU Colloquium 164: Radio Emission from Galactic and Extragalactic Compact Sources, ed. J. A. Zensus, G. B. Taylor, & J. M. Wrobel, ASP Conf. Ser., 144, 279
- Parijskij, Yu. 1993, IEEE Antennas Propagation Magazine (IAPM), 35, 7
- Pauliny-Toth, I. I. K., Witzel, A., Preuss, E., Baldwin, J. E., & Hills, R. E. 1978, A&AS, 34, 253
- Perley, R., & Taylor, G. 1999, VLA Calibrator Manual, <http://www.nrao.edu/~gtaylor/calibr.html>
- Rengelink, R. B., Tang, Y., de Bruyn, A. G., et al. 1997, A&AS, 124, 259
- Trushkin, S. 1985, Ph.D. Thesis, Special Astrophysical Observatory of Russian Academy of Sciences
- Verkhodanov, O., Trushkin, S., Andernach, H., & Cherenkov, V. 1997, The CATS database to operate with astrophysical catalogs, in Astronomical Data Analysis Software and Systems VI, ed. G. Hunt, & H. E. Payne, ASP Conf. Ser., 125, 322
- Verkhodanov, O. 1997, Multiwaves continuum data reduction at RATAN-600, in Astronomical Data Analysis Software and Systems VI, ed. G. Hunt, & H. E. Payne, ASP Conf. Ser., 125, 46
- de Vries, W. H., Barthel, P. D., & O'Dea, C. P. 1997, A&A, 321, 105